IEEE Photonics Journal
An IEEE Photonics Society Publication

Open Access

Visualization of Spatial–Temporal Evolution of Light-Induced Refractive Index in Mn:Fe:KTN Co-Doped Crystal Based on Digital Holographic Interferometry

Volume 7, Number 4, August 2015

Qieni Lu
Jinxin Han
Haitao Dai
Baozhen Ge
Shuang Zhao

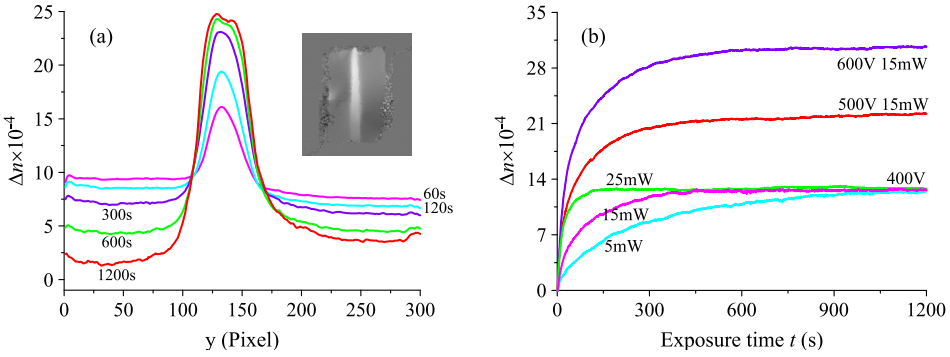

DOI: 10.1109/JPHOT.2015.2438444
1943-0655

Visualization of Spatial–Temporal Evolution of Light-Induced Refractive Index in Mn:Fe:KTN Co-Doped Crystal Based on Digital Holographic Interferometry

Qieni Lu,[1,2] Jinxin Han,[1,2] Haitao Dai,[3] Baozhen Ge,[1,2] and Shuang Zhao[1,2]

[1]School of Optoelectronics & Precision Instrument Engineering, Tianjin University, Tianjin 300072, China
[2]Key Laboratory of Opto-electronics Information Technology, Ministry of Education, Tianjin 300072, China
[3]School of Science, Tianjin University, Tianjin 300072, China

DOI: 10.1109/JPHOT.2015.2438444

Manuscript received April 28, 2015; revised May 19, 2015; accepted May 22, 2015. Date of publication June 12, 2015; date of current version June 23, 2015. This work was supported by the National Natural Science Foundation of China under Grant 61077072. Corresponding author: Q. Lu (e-mail: qienil@tju.edu.cn).

Abstract: The dynamic refractive-index-change behavior of the light-induced process in an Mn:Fe:KTN crystal illuminated by a focused light sheet can be observed experimentally by digital holographic interferometry. By numerically retrieving a series of sequential phase maps from recording digital holograms, the spatial and temporal evolution of the light-induced refractive-index-change distribution inside the material is visualized *in situ* and monitored in a quantitative and in full field way. With this technique, the effect of recording parameters, such as writing laser power and polarization, bias voltage, temperature, and writing time, on the Mn:Fe:KTN crystal in the photorefractive effect can be explored. Therefore, optimized recording parameters will be achieved according to the dynamic behavior. The method provides an access to explore the evolution of the photorefractive (PR) effect of electrooptic crystal under various situations.

Index Terms: Mn:Fe:KTN crystal, photorefractive (PR) effect, digital holographic interferometry.

1. Introduction

The photorefractive (PR) effect, i.e., light-induced refractive index change, which converts the variations of light intensity dynamically to changes in refractive index, has attracted intense attention and been intensively investigated for about decades since Ashkin *et.al* first observed the phenomenon [1]–[7]. Potassium tantalate niobate (KTN) crystal is one of the first identified crystal with PR effect and known also with a very large second-order electro-optic (EO) effect [8]–[10], which has thus been substantially investigated [11]–[13], and applied in many fields such as holographic storage [14], EO deflection [15], [16], a fast varifocal lens [17], [18]. A Mn:Fe:KTN crystal doped with both iron and manganese is particularly interesting because it has two competing subsystems of dipole moments, which exhibits higher EO performance, such as, higher diffractive efficiency and PR sensitivity and faster response time. Therefore, the learning and manipulating of photorefractive process matters to read the exact temporal and

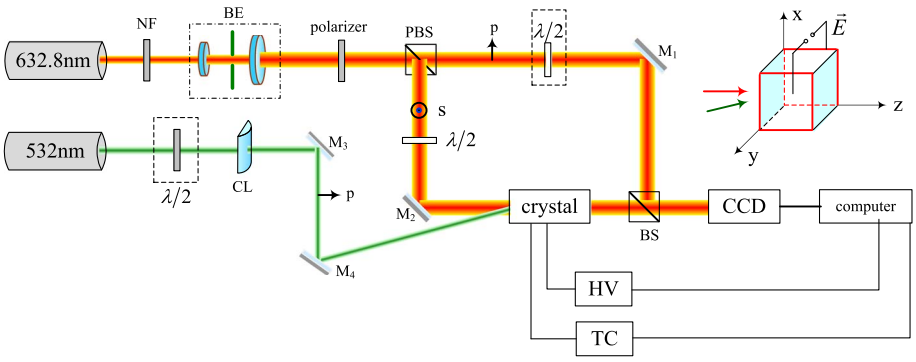

Fig. 1. Experimental optical setup for measurement of refractive index changes. The refractive index is induced by illumination with a focused laser beam (NF: a variable neutral density filter; BE: beam expander, spatial filter, and collimator; PBS: polarizing beam splitter; BS: beam splitter; M_1–M_4: mirror; $\lambda/2$: half-wave plate; HV: high-voltage power supply; TC: temperature control system; CL: cylindrical lens).

spatial behavior of the refractive index change in the material. Several techniques have been suggested for this purpose. For example, digital holography has been presented for *in situ* observation of the light-induced refractive index change in a $LiNbO_3$: Fe sample, by which the phase map of the optical path difference can be obtained due to the refractive index changes [19], [20]. The optical interferometric technique has been applied in visualizing the light-induced changes of refractive index of a $LiNbO_3$:Fe sample in [6] and [7]. However, little attention has been paid to visualizing simultaneously the spatial and temporal evolution of the light-induced refractive index change of a photorefractive crystal under an electric field, and the time evolution is important to evaluate PR processing, specifically for PR solitons, observing the process of soliton information in crystal. In this paper, we utilize digital holographic interferometry to visualize the characteristics of the spatial and temporal behavior of light-induced refractive index change and monitor the refractive index change quantitatively in Mn:Fe:KTN crystal. The method is used simultaneously to observe the light-induced refractive index change in Mn:KLTN (potassium lithium tantalate niobate) crystal [21]. However, some different characteristics of light-induced refractive index change in Mn:Fe:KTN crystal are observed just as we expected, which is intriguing and significant, and those result from those different mechanisms, the one-center model and the two-center model, which are responsible for single and double doped in crystal, respectively. Here off-axis holographic system is also involved, which can record holograms of a Mn:Fe:KTN crystal, retrieve the phase distortions under different states and visualize the optical field distribution of the Mn:Fe:KTN crystal illuminated by focused vertical light *in situ*. And the temporal evolution of the reduced refractive index change is estimated by means of a series of sequential phase difference.

2. Experimental Setup and Method

The experimental configuration for studying spatial and temporal behavior of light-induced refractive index change in a KTN crystal is illustrated schematically in Fig. 1, which consists of two setups: the inducing optical setup and the probing optical setup as we call it here. For the inducing optical setup, a 532 nm continuous-wave (cw) horizontally linearly polarized semiconductor laser with the maximum power of 100 mW is adopted as a writing light source, and a laser beam is focused by a cylindrical lens to approximate a vertical 0.3 mm sheet to induce a refractive index change. A $\lambda/2$ wave plate with $\lambda = 532$ nm is used to change extraordinary polarized light to ordinary polarized light. The spatial distribution and temporal evolution of the optically induced change of the index of refraction is probed by digital holographic interferometry in the probing optical setup, which is a Mach-Zehnder-like holographic arrangement. A linearly polarized light from a He-Ne laser (Thorlabs HNL050L) with the wavelength of 632.8 nm

serves as a probe light source and is expanded, spatially filtered, and collimated. Then, the plane wave with the diameter 20 mm is divided into two parts, which have the same intensity, through a polarizing beam splitter cube PBS and a polarizer. The horizontally linearly polarized light, namely, p-polarized light, reflected by reflecting mirror M_1 and beam splitter cube BS, acts as the reference wave; the vertically linearly polarized light, that is s-polarized light, is reflected by reflecting mirror M_2 and illuminate the object and through BS onto the CCD plane, as the object wave. A half-wave plate ($\lambda/2$, here $\lambda = 632.8$ nm) is inserted in the object arm or in the reference arm to permit selection of p-polarized light or s-polarized light. And the two beams are interfering and a Fresnel off-axis hologram is formed and recorded on a CCD. The CCD used is a 14-bit digital CCD camera (GRAS-14S5M/C) with 1384 $\times$ 1036 pixels and pixel size of 6.45 μm $\times$ 6.45 μm. The Mn:Fe:KTN, with $Mn_{0.04}$:$Fe_{0.15}$:$KTa_{0.60}Nb_{0.40}O_3$, is grown by the top-seed solution growth method, used as the object. The temperature of the sample in the experiment is controlled by a temperature control system (TC) we developed with a precision of 0.5 °C. DC electric field is applied to the sample by a high-voltage power supply (Agilent N5772A). In the experiment, to avoid the probe beam producing additional index changes in the crystal, the He-Ne laser is operated at much lower power by NF.

Let $I_1(x, y)$ and $I_2(x, y)$ be the digital holograms recorded in two different states of the object, and $o_1(x, y)$ and $o_2(x, y)$ be the reconstructed complex amplitude of object wave from $I_1(x, y)$ and $I_2(x, y)$, and the corresponding phase distribution $\varphi_1(x, y)$ and $\varphi_2(x, y)$, respectively, are given by

$$\varphi_i(x, y) = \arctan\frac{\mathrm{Im}o_i(x, y)}{\mathrm{Re}o_i(x, y)} \quad i = 1, 2. \tag{1}$$

The phase difference of object in two different states, called the interference phase, can be written as

$$\delta(x, y) = \begin{cases} \varphi_1(x, y) - \varphi_2(x, y) & \varphi_1(x, y) \geq \varphi_2(x, y) \\ \varphi_1(x, y) - \varphi_2(x, y) + 2\pi & \varphi_1(x, y) < \varphi_2(x, y). \end{cases} \tag{2}$$

The refractive index change $\Delta n(x, y)$ between two exposures, which observed is attributed to the intense laser illumination, is proportional to the phase difference, which is calculated by

$$\Delta n(x, y) = \frac{\lambda\delta(x, y)}{2\pi d} \tag{3}$$

where λ is wavelength, and d is thickness of crystal in laser beam propagating direction (z-direction). The phase map representing the phase change directly reflects the variation of refractive index of KTN crystal by photorefractive effect. Therefore, the photorefractive effect of KTN crystal can be displayed and analyzed in the form of phase maps.

3. Experiment Results and Analysis

3.1. PR Effect

The as-grown of Mn:Fe:KTN crystal is cut into a cube with dimensions $3.4^{(x)} \times 2.0^{(y)} \times 0.94^{(z)}$ mm^3 along the crystallographic [010] axis. Both $3.4^{(x)} \times 2.0^{(y)}$ mm^2 faces are optically polished for light propagation. Silver electrodes are plated and two silver conducting wires are attached on both of the $3.4^{(x)} \times 0.94^{(z)}$ mm^2 faces, and an electric field $\vec{E}$ is applied along the y axis, that is, $\vec{E}(0, E, 0)$, by DC-voltage source. The temperature dependence of the relative dielectric constant ε_r is measured by an LCR meter (Agilent E4980A), as shown in Fig. 2. The peak of the curve indicates that the Curie temperature is $Tc = 27$ °C, and the crystal had a large relative dielectric constant near Tc. The large dielectric constants of the crystal near the phase-transition temperature will induce a large Kerr effect in the paraelectric phase. We measure the quadratic EO coefficient using digital holographic interferometry [22], and R_{11} reaches as high as

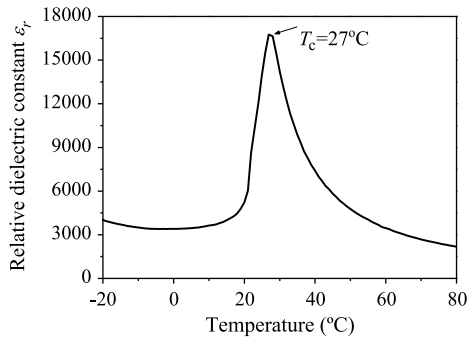

Fig. 2. Dependence of the relative dielectric constant ε_r on temperature, and the peak of the curve of $Tc = 27°C$.

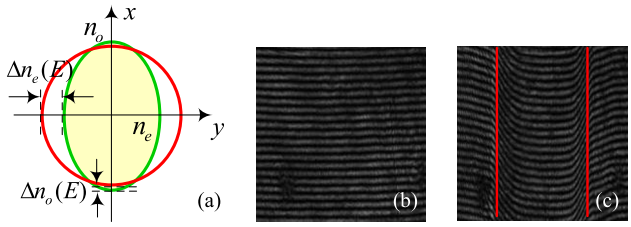

Fig. 3. (a) Intersection of the index ellipsoid with xy plane when electric field is applied along the y axis ($E = 300$ V/mm, green curve) and without the field (red curve). Holograms of the light-induced refractive index changes with the writing light and recording light of p-polarized light for (b) $U = 0$ V and (c) $U = 600$ V, temperature of 30 °C, the exposure times of 300 s, and the writing light power of 15 mW.

7.81×10^{-15} m^2/V^2 and R_{12} is -4.558×10^{-16} m^2/V^2 at 28 °C around Tc. For p-polarized light and s-polarized light, the modulation of the refractive index n_o and n_e induced by EO effect is different. Fig. 3(a) shows the intersection of the (y, x) plane with the index ellipsoid in KTN determined by the equation as follows:

$$\left(\frac{1}{n_0^2} + R_{12}\right)x^2 + \left(\frac{1}{n_0^2} + R_{12}\right)z^2 + \left(\frac{1}{n_0^2} + R_{11}\right)y^2 = 1 \tag{4}$$

where n_0 is the principal axe of the refractive index ellipsoid without electric field applied, and the electric field $\vec{E}$ is parallel with y-axis. The semiaxes of the intersection of index ellipsoid in the (y, x) plane are coincident with refractive indices of the ordinary and extraordinary polarizations of the reading beam, and the modulation of the refractive index $\Delta n_o(E) \approx -n_0^3 R_{12} E^2/2$, $\Delta n_e(E) \approx -n_0^3 R_{11} E^2/2$. The value n_e of TM mode is larger than that n_o of the TE mode. For comparison, the intersection with no electric field applied is also drawn in Fig. 3(a), in which KTN crystal in the paraelectric phase is isotropic. When the high power focused Gaussian light sheet illuminates the sample, the induced index change Δn_o and Δn_e by PR effect are also different. Fig. 3(b) and (c) show the digital holograms obtained by the recording magnification interference field in the absence and in the presence of applied voltage, respectively, for writing light and recoding light are the p-polarized light. The interference fringes change occurs in Fig. 3(c), and there is no change in $(n_o - n_e)$ in Fig. 3(b) when illuminated if no electric filed is supplied, the result of which verified the conclusion that the light-induced refractive index change can be explained by a result of the EO effect. Fig. 4(a)–(c) show holograms with and without the p-polarized writing light for the p and s-polarized recoding light, respectively. Fig. 4(d)–(f) show holograms with and without the s-polarized writing light for the p and s-polarized recoding light, respectively. The experimental parameters used follow: voltage of 600 V, temperature of 30 °C,

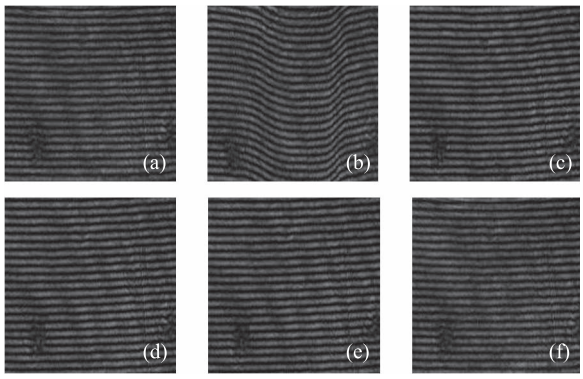

Fig. 4. Holograms of the light-induced refractive index changes at 600 V, 100 s, and 30 °C. (a) p-polarized recoding light and no writing light. (b) p-polarized writing light and the p-polarized recoding light. (c) p-polarized writing light and the s-polarized recoding light. (d) s-polarized recoding light and no writing light. (e) s-polarized writing light and the s-polarized recoding light. (f) s-polarized writing light and the p-polarized recoding light [the illumination region is the same as in Fig. 3(c)].

the exposure times of 100 s, and the writing light power of 15 mW. The shift of the interference fringes in the illumination region (red curve marks the illumination region) show that the illumination by a Gaussian light sheet really induces changes of the refractive index, while the shift of the interference fringes in the illuminated region shown in Fig. 4(c), (e), and (f) are too small or show almost no shift to be observed by the naked eye at the present voltage applied. Those results imply that the refractive index change occurs only when the writing laser beam and electric field are simultaneously present, and the magnitude of the refractive index change in the crystal depends on the appropriate EO coefficients. With n_o little affected, only Δn_e is then considered. In our experiment, a voltage is always applied to the Mn:Fe:KTN crystal tested, the probe light and the writing light are p-polarized light, the writing light enters the Mn:Fe:KTN crystal centered to the middle of the surface whose direction of propagation is 5° along to the z axis, the very small angle between the probe light and the writing light occurs due to the border of reflecting mirror M_2, only part of the surface of the crystal is illuminated. Experiments are conducted with respect to variations in writing light intensity, applied voltage, temperature, and exposure time. The phase changes of the crystal during and after illumination, i.e., between the exposure time $t \neq 0$ s and $t = 0$ s, are visualized and measured.

3.2. Under a Constant Temperature

The experimental procedure for measuring the light-induced birefringence is based on determining the phase map through the crystal. For this end, we first carry out the experiment under a constant temperature of 30 °C, 3 °C above its Curie temperature. Digital holograms of the crystal at various levels of writing-beam power, bias field strengths and exposure times are recorded and numerically reconstructed by angular spectrum method [23], the phase differences of object in two different states are extracted using (1) and (2), and filtered by median filter and unwrapped by 3D unwrapping algorithm [24]. The phase changes of the crystal between the exposure time $t \neq 0$ s and $t = 0$ s are measured. Fig. 5(a)–(f) show the partial phase map of the crystal with the exposure times of 30 s, 60 s, 180 s, 300 s, 600 s, 1200 s, voltage of 600 V and laser power of 15 mW, respectively. Fig. 6 shows a frame of the movie obtained collecting 200 of the three-dimensional phase map during the exposure time of 5 min (Media 1), and the phase retardation can be visualized and observed. It is clearly seen from Figs. 5 and 6 that the phase amplitude increases as the exposure time lengthens. The same results are also observed in Figs. 3(c) and 4(b). According to (3), the phase difference distribution measured $\delta(x, y)$ is converted to the induced refractive index change $\Delta n(x, y)$, and the temporal evolution of the refractive index changes is estimated. Fig. 7 gives the spatial variation of $\Delta n(x, y)$ along the y axis

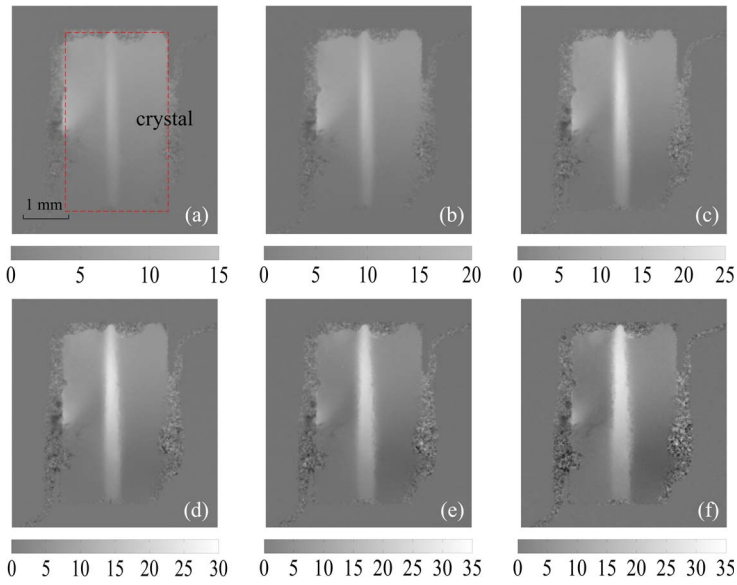

Fig. 5. Spatial-temporal evolution of the phase field. (a) $t = 30$ s. (b) $t = 60$ s. (c) $t = 180$ s. (d) $t = 300$ s. (e) $t = 600$ s. (f) $t = 1200$ s. (The color bar corresponds with the phase value (rad) of the marked area.)

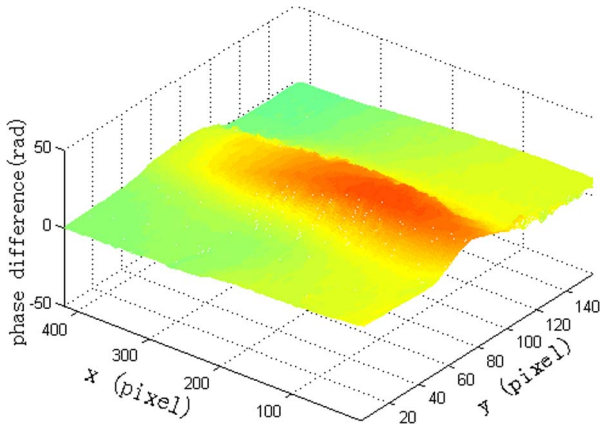

Fig. 6. Dynamic behavior of phase retardation for exposure time of 5 min (Media 1).

for various exposure times with voltage of 500 V and laser power of 15 mW. It can be observed that the induced index changes $\Delta n(x, y)$ are practically restricted within the beam region (see Figs. 3–7). With longer exposure time, $\Delta n(x, y)$ subsequently reaches a steady state, for example, the value of $\Delta n(x, y)$ for the exposure time of 600 s is almost the same as that of 1200 s. The averaged value Δn of $\Delta n(x, y)$ is used for the following analysis.

Fig. 8(a) shows the average Δn with respect to exposure time t for different voltages U and a fixed power of 15 mW. Fig. 8(b) plots the average Δn as a function of laser power I and exposure time t at a fixed electric field of 400 V. One can see from Fig. 8, Δn increases with exposure times t, when the beam power I incidents on the Mn:Fe:KTN crystal and exposure time t are kept at the same level, Δn increases with increasing voltage. Similarly, when the applied voltage U and exposure time t are kept at the same level, Δn rises at a higher beam power I. Subsequently, it saturates after a certain exposure time, and the saturation value of the refractive-index changes Δn_s depends on the applied electric field, and increases as the electric field strengthens, which differs from the result of Mn:KLTN crystal in [21]. The phenomenon in

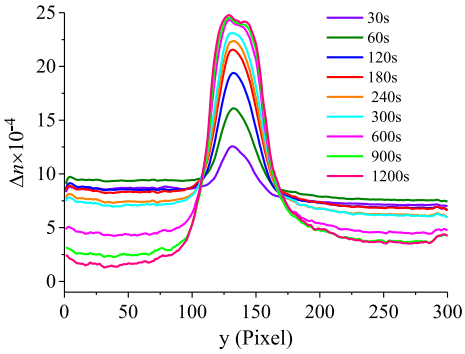

Fig. 7. Refractive index changes Δn with various exposure times (at $x = 390$ pixels; see Fig. 6).

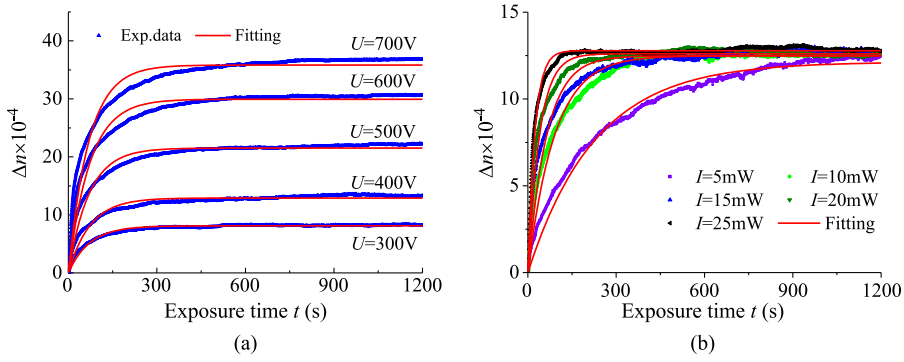

Fig. 8. Average Δn as a function of exposure time. (a) For various applied voltages at a fixed power of 15 mW, (b) for different focused light power at a fixed applied voltage of 400 V.

Fig. 8 is explainable with the two-center model of Kukhtarev *et al.* [25], and the writing time constant t_w and Δn_s have been obtained by fitting the $\Delta n - t$ curves shown in Fig. 8 to the function

$$\Delta n = \Delta n_s[1 - \exp(-t/t_w)] \tag{5}$$

The fitting results are shown as red solid lines in Fig. 8(a) and (b), the red solid fitting curves coincide with the experiment data profile, and the fitting parameters are listed in Tables 1 and 2. Form Tables 1 and 2, you notice that t_w can be seen as a constant for the voltage of 300 V–700 V at the same light intensity I, the average $t_w = 70.684$ s for the light power of 15 mW, which indicates t_w is a function of the incident light intensity I, and the value of t_w determines the build-up time of the refractive-index changes Δn. While the saturation value Δn_s is dependent on the electric field U but not on the incident light intensity I, which increases with rising voltage.

The laser power dependence of the writing time is also investigated. The writing time constant $t_w = \varepsilon_r \varepsilon_0 / 4\pi\sigma_{ph}$, where ε_0 is the vacuum permittivity, ε_r is the relative permittivity and σ_{ph} is the photoconductivity. According to the photoconductivity $\sigma_{ph} \propto I^x$ [26], then we can obtain $t_w = aI^{-x}$, where a is the scale coefficient. From Table 2, we get the fitted equation of the writing time constant $t_w = 1.759 \times 10^3 I^{-1.265}$ using the light power of 5, 10, and 20 mW, which is tested by the light intensity of 15 and 25 mW. The writing time constant t_w obtained by $t_w = 1.759 \times 10^3 I^{-1.265}$ are 57.215 s and 29.983 s and 61.333 s and 24.533 s from the experiments, respectively, the results of which are in agreement.

From above analysis, to obtain high value of Δn_s and the short t_w, the optimized recording parameters, as we take it, can be selected as the following procedure in PR process. The high

TABLE 1

Fitting parameters t_w and Δn_s of curve shown in Fig. 8(a)

voltage U(V)	laser power I(mW)	writing time constant t_w(s)	saturation value $\Delta n_s \times 10^{-4}$
300	15	71.131	7.570
400	15	72.950	12.045
500	15	69.881	20.074
600	15	72.676	27.933
700	15	69.301	33.424

TABLE 2

Fitting parameters t_w and Δn_s of curve shown in Fig. 8(b)

voltage U(V)	laser power I(mW)	writing time constant t_w(s)	saturation value $\Delta n_s \times 10^{-4}$
400	5	229.691	12.137
400	10	90.482	12.492
400	15	68.164	12.482
400	20	39.767	12.608
400	25	23.586	12.784

electric field to be applied should be determined first with the crystal breakdown voltage and the power consumption taken into account; the high light intensity should then be utilized with scatter another factor considered, the writing light and the recoding light are both p-polarized light, and the exposure time is about 1.5 times t_w given by fitted equation.

3.3. Under Different Temperatures

The phase transition for Mn:Fe:KTN occurs at around $Tc = 27$ °C. Above Tc, the crystal is in the cubic phase, which is the quadratic EO effect, and below Tc, it is in the tetragonal phase, which is the linear EO effect. The same system and method of visualization and measurement of light-induced refractive index changes mentioned in Section 3.2 are used in this experiment. In our experiment, the temperature of the sample is controlled by a temperature control system (TC). In light of the results of our investigation in Section 3.2, the optimized recording parameters we set are the writing laser power of 15 mW, the applied voltage 300 V/mm, i.e., 600 V, and the exposure time 100 s. Fig. 9(a)–(f) show the unwrapped phase difference between exposure time $t = 100$ s and $t = 0$ s with at 24, 26–29, and 31 °C, respectively. Fig. 10(a) and (b) respectively depict the dependence of the average Δn on exposure time under temperature above Tc and below Tc, which are the temporal evolution of the phase difference or the refractive index change. Similarly, Fig. 10 is fitted by (5) as well, one can notice that the red solid fitting curves in Fig. 10 match the experiment data profile in all data for 21–33 °C except 27 °C. And it is clearly seen from Figs. 9 and 10 that the phase amplitude and the refractive index change increase from 23 °C to 26 °C and decrease from 28 °C to 33 °C as temperature rises, and the peak value of Δn appears at 27 °C, which is the Curie temperature. Theoretically, Δn does not have a saturation value at 27 °C and yet does not satisfy (5). Fig. 11(a) and (b) plot the saturation value of Δn_s and the writing time constant t_w as function of temperature T, respectively. Black dots in Fig. 11(a) and (b) marked as the experiment data agrees with the fitting data except 27 °C, specifically the writing time constant t_w, and the variation distribution of Δn_s with temperature T is very similar to that of the dependence of the dielectric constant on temperature T, which satisfies the Curie-Weiss law.

4. Conclusion

We successfully visualize the dynamic behavior of the refractive index change distribution of EO crystal in the photorefractive process with digital holographic interferometry *in situ*. Quantitatively,

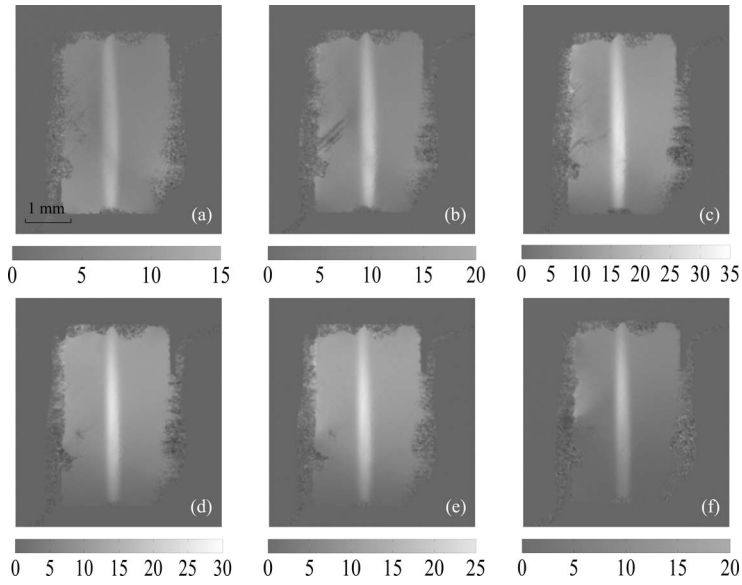

Fig. 9. Unwrapped phase difference at the different temperatures. (a) $T = 24$ °C. (b) $T = 26$ °C. (c) $T = 27$ °C. (d) $T = 28$ °C. (e) $T = 29$ °C. (f) $T = 31$ °C. (The color bar is the same as in Fig. 5.)

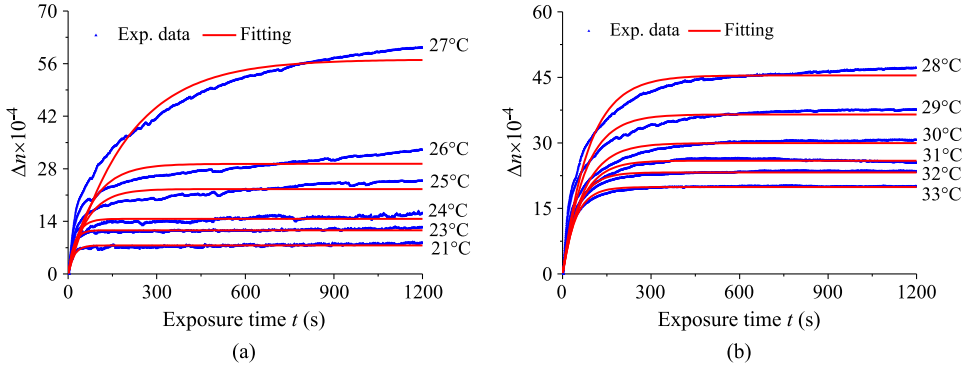

Fig. 10. Average Δn with respect to exposure times. (a) $T < Tc$. (b) $T > Tc$.

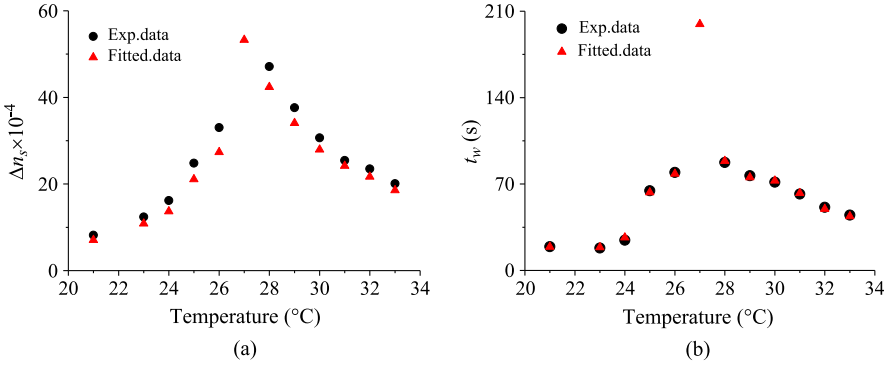

Fig. 11. Temperature dependence of (a) the saturation value of Δn_s amplitude and (b) the writing time constant t_w of refractive index change.

we measure spatial and temporal response of 2-D refractive index distribution in a Mn:KLTN crystal and Mn:Fe:KTN crystal after exposure, and the optimized recording parameters are achieved. The research results demonstrate visualization and quantitative phase measurement by the experimental method presented is a promising technique for the investigation of PR process. Compared with Mn:KLTN crystal, the Mn:Fe:KTN crystal has large refractive index change at the same voltage, which means that the large Δn_s can be obtained in the co-doped crystal with the driving voltage of the crystal used effectively lowered, and the longer storage time is obtained. Moreover, a sound writing condition is achieved for the grating formed by PR process, which can highly helpful for electroholographic switching, still under our further exploration.

Acknowledgment

The authors would like to thank Prof. Z. Zhongxiang and Prof. T. Hao, as well as their research group at the Department of Physics, Harbin Institute of Technology, for their help in the crystal growth and sample preparation.

References

[1] A. Ashkin *et al.,* "Optically-induced refractive index inhomogenities in $LiNbO_3$ and $LiTaO_3$," *Appl. Phys. Lett.*, vol. 9, no. 1, pp. 72–74, Jul. 1966.
[2] F. S. Chen, "Optically induced change of refractive indices in $LiNbO_3$ and $LiTaO_3$," *J. Appl. Phys.*, vol. 40, no. 8, pp. 3389–3396, Jul. 1969.
[3] N. Sapiens, A. Weissbrod, and A. J. Agranat, "Fast electroholographic switching," *Opt. Lett.*, vol. 34, no. 4, pp. 353–355, Feb. 2009.
[4] A. Gumennil, G. Perepelitsa, A. Israel, and A. J. Agranat, "A tunable channel waveguide array fabricated by the implantation of He^+ ions in an electrooptical KLTN substrate," *Opt. Exp.*, vol. 17, no. 8, pp. 6166–6167, Apr. 2009.
[5] D. Pierangeli *et al.,* "Photorefractive light needles in glassy nanodisordered KNTN," *Opt. Lett.*, vol. 39, no. 6, pp. 1657–1670, Mar. 2014.
[6] I. Turek and N. Tarjányi, "Investigation of symmetry of photorefractive effect in $LiNbO_3$," *Opt. Exp.*, vol. 15, no. 17, pp. 10 782–10 788, Aug. 2007.
[7] K. Peithmann, A. Wiebrock, K. Buse, and E. Krätzig, "Low-spatial-frequency refractive-index changes in iron-doped lithium niobate crystals upon illumination with a focused continuous-wave laser beam," *J. Opt. Soc. Amer. B, Opt. Phys.*, vol. 17, no. 4, pp. 586–592, Apr. 2000.
[8] F. S. Chen, "A laser-induced inhomogeneity of refractive indices in KTN," *J. Appl. Phys.*, vol. 38, pp. 3418–3420, Mar. 1967.
[9] Y.-C. Chang, C. Wang, S. Yin, R. C. Hoffman, and A. G. Mott, "Giant electro-optic effect in nanodisordered KTN crystals," *Opt. Lett.*, vol. 38, no. 22, pp. 4574–4577, Nov. 2013.
[10] D. Pierangeli *et al.,* "Observation of an intrinsic nonlinearity in the electro-optic response of freezing relaxors ferroelectrics," *Opt. Mater. Exp.*, vol. 4, no. 8, pp. 1487–1493, Jul. 2014.
[11] F. Di Mei *et al.,* "Anti-diffracting beams through thediffusive optical nonlinearity," *Opt. Exp.*, vol. 22, no. 25, pp. 31 434–31 439, Dec. 2013.
[12] L. Wang *et al.,* "Field-induced enhancement of voltage-controlled diffractive properties in paraelectric iron and manganese co-doped potassium-tantalite-niobate crystal," *Appl. Phys. Exp.*, vol. 7, no. 11, Oct. 2014, Art. ID. 112601.
[13] H. Tian, B. Yao, C. P. Hu, X. D. Meng, and Z. X. Zhou, "Impact of polar nanoregions on the quadratic electro-optic effect in $K_{0.95}Na_{0.05}Ta1_{-x}Nb_xO_3$ crystals near the Curie temperature," *Appl. Phys. Exp.*, vol. 7, no. 6, May 2014, Art. ID. 062601.
[14] A. Agranat, V. Leyva, and A. Yariv, "Voltage-controlled photorefractive effect in paraelectric $KTa_{1-x}Nb_xO_3$:Cu, V," *Opt. Lett.*, vol. 14, no. 18, pp. 1017–1019, Sep. 1989.
[15] T. Imai, J. Miyazu, and J. Kobayashi, "Charge distributions in $KTa_{1-x}Nb_xO_3$ optical beam deflectors formed by voltage application," *Opt. Exp.*, vol. 22, no. 12, pp. 14 114–14 126, Jun. 2014.
[16] J. Miyazu *et al.,* "New beam scanning model for high-speed operation using $KTa_{1-x}Nb_xO_3$ crystals," *Appl. Phys. Exp.*, vol. 4, no. 11, Oct. 2011, Art. ID. 111501.
[17] T. Inagaki, T. Imai, J. Miyazu, and J. Kobayashi, "Polarization independent varifocal lens using KTN crystals," *Opt. Lett.*, vol. 38, no. 15, pp. 2673–2675, Aug. 2013.
[18] T. Imai *et al.,* "Fast response variable focal-length lenses using $KTa_{1-x}Nb_xO_3$ crystals," *Appl. Phys. Exp.*, vol. 4, no. 2, Feb. 2011, Art. ID. 022501.
[19] M. de Angelis, S. De Nicola, A. Finizio, and G. Pierattini, "Digital-holography refractive-index-profile measurement of phase gratings," *Appl. Phys. Lett.*, vol. 88, no. 11, Mar. 2006, Art. ID. 111114.
[20] J. L. Zhao *et al.,* "Visualization of light-induced refractive index changes in photorefractive crystals employing digital holography," *Chin. Phys. Lett.*, vol. 10, no. 20, pp. 1748–1751, Apr. 2003.
[21] J. X. Han, Q. N. Lu, H. T. Dai, S. Zhao, and Y. M. Zhang, "In situ visualizing the evolution of the light-induced refractive index change of Mn:KLTN crystal with digital holographic interferometry," *AIP Adv.*, vol. 5, no. 4, Apr. 2015, Art. ID. 047145.
[22] Q. N. Lu, S. Zhao, H. T. Dai, and Y. M. Zhang, "Simultaneous visualization of a paraelectric Mn:KNTN crystal and measurement of its Kerr coefficient by digital holographic Interferometry," *IEEE J. Photon.*, vol. 6, no. 1, Jan. 2014, Art. ID. 2600110.

[23] L. Yu and M. K. Kim, "Wavelength-scanning digital interference holography for tomographic three-dimensional imaging by use of the angular spectrum method," *Opt. Lett.*, vol. 30, no. 16, pp. 2092–2094, Aug. 2005.
[24] G. Pedrini, W. Osten, and M. E. Gusev, "High-speed digital holographic interferometry for vibration measurement," *Appl. Opt.*, vol. 45, no. 15, pp. 3456–3462, May 2006.
[25] N. V. Kukhtarev, V. B. Markov, S. G. Odulov, M. S. Soskin, and V. L. Vinetskii, "Holographic storage in electrooptic crystals. I. steady state," *Ferroelectrics*, vol. 22, no. 3/4, pp. 949–960, Aug. 1979.
[26] F. Jermann and J. Otten, "Light-induced charge transport in $LiNbO_3$:Fe at high light intensities," *J. Opt. Soc. Amer. B, Opt. Phys.*, vol. 10, no. 11, pp. 2085–2092, Nov. 1993.